Steiner, A. K., G. Kirchengast, B. C. Lackner, B. Pirscher, M. Borsche, and U. Foelsche (2009), Atmospheric temperature change detection with GPS radio occultation 1995 to 2008, Geophys. Res. Lett., 36, L18702, doi:10.1029/2009GL039777.

Atmospheric Temperature Change Detection with GPS Radio Occultation 1995 to 2008

A. K. Steiner, G. Kirchengast, B. C. Lackner, B. Pirscher, M. Borsche, U. Foelsche
Wegener Center for Climate and Global Change (WegCenter) and Institute for Geophysics, Astrophysics, and Meteorology (IGAM), University of Graz, Graz, Austria
andi.steiner@uni-graz.at
gottfried.kirchengast@uni-graz.at

Submitted to *Geophys. Res. Lett.* June 2009; revised August 2009; accepted 26 August 2009

Abstract. Existing upper air records of radiosonde and operational satellite data recently showed a reconciliation of temperature trends but structural uncertainties remain. GPS radio occultation (RO) provides a new high-quality record, profiling the upper troposphere and lower stratosphere with stability and homogeneity. Here we show that climate trends are since recently detected by RO data, consistent with earliest detection times estimated by simulations. Based on a temperature change detection study using the RO record within 1995–2008 we found a significant cooling trend in the tropical lower stratosphere in February while in the upper troposphere an emerging warming trend is obscured by El Niño variability. The observed trends and warming/cooling contrast across the tropopause agree well with radiosonde data and basically with climate model simulations, the latter tentatively showing less contrast. The performance of the short RO record to date underpins its capability to become a climate benchmark record in the future.

1. Introduction

Anthropogenic climate change manifests itself not only as warming of the Earth's surface but also as temperature change in the free atmosphere. Increasing greenhouse gas concentrations cause a warming of the troposphere whereas they cool the lower stratosphere in combination with less shortwave heating due to ozone depletion [*Baldwin et al.*, 2007]. Detection of climate change in the atmosphere requires high quality observations. Intensive efforts have been undertaken to understand and reconcile differences of temperature trends stemming from different observations and climate models [*Karl et al.*, 2006]. Radiosonde and operational satellite data now show general agreement in tropospheric warming and in stratospheric cooling being broadly consistent with surface temperature trends and climate model trends [*Santer et al.*, 2008], provided the models include transient ozone representation [*Shindell*, 2008]. Despite updated data products, disparities in quantitative trends remain due to structural uncertainties [*Titchner et al.*, 2009] since neither of the instruments was designed for climate monitoring purposes [*Randel et al.*, 2009].

RO measurements based on signals from Global Positioning System (GPS) satellites provide an independent upper air record delivering high-quality observations in the upper troposphere and lower stratosphere (UTLS) with global coverage, essentially all-weather capability and consistency [*Kursinski et al.*, 1997]. Also, traceability to the international definition of the second enables RO data to serve as climate benchmark [*Leroy et al.*, 2006a] and allows long-term measurement stability. Vertical profiles of atmospheric parameters such as bending angle, refractivity, pressure, and temperature are retrieved with high accuracy (temperature RMS errors <1 K) and vertical resolution (~0.5–1 km) in the UTLS [*Kursinski et al.*, 1997; *Rocken et al*., 1997; *Steiner et al*., 1999]. RO data from different sensors and occultation missions can be combined without inter-calibration and overlap when using consistent processing [*Hajj et al*., 2004; *Foelsche et al*., 2009; *Ho et al*., 2009]. The climate utility of RO has been demonstrated with a range of studies [e. g., *Borsche et al*., 2007; *Steiner et al*., 2007; *Schmidt et al*., 2008; *Foelsche et al*., 2009; *Ho et al*., 2009] and with observing system simulations for climate monitoring and modeling [*Leroy et al*., 2006b; *Foelsche et al*., 2008; *Ringer and Healy*, 2008]. Because of the relatively short records used there, the value of RO for long-term climate trend monitoring could not yet be definitely demonstrated until this study.

2. Data and Methods

We investigated to what degree significant trends are already detectable in RO temperatures and how trends start to exceed natural variability. First GPS RO data are available from the GPS/Meteorology (GPS/Met) proof-of-concept mission intermittently within the years 1995–1997. From September 2001 to September 2008 RO data (about 150 atmospheric profiles per day) are near-continuously available from the CHAllenging Minisatellite Payload for geoscientific research (CHAMP) mission, complemented and continued by other missions. We investigate the GPS/Met and CHAMP data within 1995–2008. Since GPS/Met provides sufficient observations of CHAMP-like quality ("Prime Time" data [*Rocken et al*., 1997]) only for October 1995 and February 1997 we focus on RO monthly-mean records for February (1997 and 2002−2008) and October (1995 and 2001−2007), respectively. We test the trend detection capability over 10–13 year periods based on zonal-mean temperature climatologies within 50°N–

50°S in the UTLS between 300–30 hPa (~9–25 km), where the data quality is best due to favorable error characteristics. Investigated are the upper troposphere (300–200 hPa; UT), tropopause region (200–100 hPa; TP), and lower stratosphere (100–30 hPa; LS) in the tropics (20°S–20°N) and Northern/Southern hemisphere extratropics (20°N–50°N/20°S–50°S; NHE/SHE). A method summary and a detailed description of data sets, computation procedures, and applied statistical methods is given in the auxiliary material[1].

The results are compared to trends in the radiosonde temperature record and in global climate model (GCM) runs. We use radiosonde data from the Hadley Centre/MetOffice, UK (HadAT2) [*Thorne et al*., 2005; *Titchner et al.*, 2009] and newly homogenized records from the University of Vienna, Austria (RICH) [*Haimberger et al*., 2008]. We also employ an ensemble of runs of three representative GCMs used for the Intergovernmental Panel on Climate Change Fourth Assessment Report (IPCC AR4): NCEP-NCAR/CCSM3, MPI/ECHAM5, and UKMO/HadCM3 (auxiliary Table S1).

3. Results

Figure 1 shows RO temperature anomalies and linear trends for February 1997–2007 and 1997–2008 (Figure 1a, d, g) (discussed in context with Figure 2 below), which were calculated by considering the individual total error for each month (Figure 1b, e, h), which in turn is composed of the residual sampling error, the observation error, and a systematic error bound (Figure 1c, f, i). The residual sampling error was conservatively adopted as 50 % of the estimated sampling error that was subtracted. The observation error results from the individual profile statistical error (~1 K) divided by the square root of the number of profiles in the respective region (Table S2). A (time-varying) systematic error bounded to 0.2 K above 100 hPa and to 0.1 K below was conservatively assumed in line with estimates of potential residual biases. The total error of ~0.5 K for GPS/Met data in February 1997 in the NHE UT (Figure 1b) is dominated by the residual sampling error (Figure 1c). The same largely applies to CHAMP data in the NHE, whereas in the tropics the systematic error dominates (Figure 1e). October 1995–2007 temperatures show similar error characteristics (Figure S1). The sampling error dominates if a smaller number of RO observations is available and in case of higher atmospheric variability (hemispheric winter; NH in February, SH in October).

Figure 2 presents climate variability, trends, and their significance for February 1997–2008 for the investigated regions and height layers. The inter-annual climate variability (represented by the de-trended standard deviation) and the error of the trend are used to assess the signal-to-noise ratio of the trend in the study period (autocorrelation was found negligible). We also inspect whether the trend exceeds long-term natural variability of 12-year trends in February as estimated from pre-industrial control runs of the three selected models. Each model shows different characteristics of internal variation and together they cover a best-estimate range of variability (Figure S2).

A significant cooling trend (–1.79±0.29 K/12a) was found relative to natural variability (0.63 K) at the 95 % significance level and relative to inter-annual variability (0.78 K) at the 90 % significance level in the tropical LS (Figure 1d, top). In the NHE UT a linear fit is not adequate as obvious in Figure 1a (bottom panel). Checking sensitivities, we also inspected the period February 1997–2007. Here we found the cooling trend confirmed robust in the tropical LS

[1]Auxiliary materials are available in the HTML. doi:10.1029/2009GL039777.

(95 % level) but we also found a significant warming trend in the tropical TP (95 % level) and in the tropical UT, relative to inter-annual variability (90 % level). October time series show smaller variability and smaller trends. A significant warming trend was found in the tropical UT relative to inter-annual variability (90 % level) for October 1995–2006 but the trend is not significant for 1995–2007 (Figure S3).

Thus while the LS trend appears robust, the UT trend does not and we investigated which internal climate variability may cause the sensitive behavior of the latter. Major volcanic eruptions are no candidates since none took place in the relevant years 1995, 1997, 2001–2008. The stratospheric Quasi-Biennial Oscillation (QBO) is clearly observable in RO data of the tropical LS. However, in our context the QBO pattern becomes very small since we average the LS over a large domain of 20°S–20°N and of 100 hPa–30 hPa (Figure S4). Thus it showed no important influence on the RO temperatures (Figure S5) and is disregarded hereafter. Concerning El Niño Southern Oscillation (ENSO) the relevant years are dominated by weakly pronounced El Niño conditions (warmer than average) disrupted by a minor La Niña (colder than average) event in 2005/06, and a moderate one in 2007/08. We inspected the influence of ENSO on the RO temperatures (Figure 3). Trends were calculated with multiple linear regression including ENSO represented by the monthly Nino 3.4 (N3.4) Sea Surface Temperature (SST) index. Because atmospheric temperature lags the ENSO patterns we used a lag of four months as found from RO data analysis and literature (see auxiliary material).

In the tropical LS, a significant cooling trend (–1.89±0.29 K/12a) relative to natural variability (95 % level) and to inter-annual variability (90 % level) was found, consistent with the trend estimate using standard regression (Figure 1d). About half of the inter-annual variability in the LS is explained by an ENSO-related signal (N3.4 coefficient of –0.46 K/K, Figure 3a). In the tropical UT a strong ENSO signal explains most of the inter-annual variability (N3.4 coefficient of 0.51 K/K), obscuring an emerging warming trend signal of 0.41±0.19 K/12a (Figure 3b).

Figure 4 shows tropical temperature profile trends for February 1997–2008 (a), 1997–2007 (b), and 1997–2006 (c), respectively. Since the only independent UTLS profile data set available for cross-comparison is radiosonde data, we compared the RO data to the HadAT2 and the RICH radiosonde records, and also to an ensemble of 10–12-year running trends within 2001–2020 extracted from the A2 and B1 runs of the three selected GCMs. Agreement between HadAT2 and RO data is good within uncertainty estimates. HadAT2 shows a smaller cooling trend than RO in the LS in February. Closer agreement is found for October trends which are generally smaller (Figure S6). GCMs agree in envelope as well though the bulk shows less warming/cooling contrast across the tropical tropopause. Good agreement between RICH and RO data is found for all investigated periods (Figure 4, Figure S6) except for February 1997–2008 UT trends (Figure 4a). While the uniformly distributed RO data consistently show a cooling due to the La Niña 2007/08 event (Figures 1 and 3) this seems not captured by radiosondes due to their void in the Pacific ENSO region.

Checking sensitivities, we also compared trends based on all available RO data (including GPS/Met and all CHAMP months September 2001 to February 2008) with HadAT2 trends in 10°-zonal bands and found consistent trend patterns (Figure S7). Inspecting, for context, the continuous period 1995–2008 in HadAT2 data shows coherent UT warming and LS cooling across 20°S–20°N. Disregarding GPS/Met and inspecting only the CHAMP period again reveals consistent trend patterns between RO and radiosonde data but the LS cooling trend is not significant over this short 7 years-only timeframe dominated by inter-annual variability.

4. Conclusions

RO provides an independent climate record of high quality and vertical resolution with long-term stability. We found the RO data capable to start detecting significant UTLS climate trends relative to natural variability over a 10–13 years period, consistent with expected detection times [*Leroy et al*., 2006b; *Foelsche et al*., 2008; *Ringer and Healy*, 2008]. The results are in agreement with trends in radiosonde records, especially newly homogenized ones [*Haimberger et al*., 2008], though those trends are not significant themselves given the less stable error characteristics. While the RO record grows and further gains quality and significance, closer comparison to how climate models represent the thermal structure of the tropical UTLS is of particular interest, e.g., in view of its key role in the water vapor-lapse rate feedback [*Randall et al*., 2007]. The present (limited) results tentatively indicate less UTLS warming/cooling contrast in models than in RO data. Overall the performance of the still short RO record is encouraging that it may develop into a climate benchmark record in future.

Acknowledgments. The authors acknowledge UCAR/CDAAC (Boulder, CO, USA) for GPS/Met and CHAMP phase delay and orbit data, ECMWF (Reading, UK) for analysis and forecast data, Hadley Centre/MetOffice (Exeter, UK) for HadAT2 data, and L. Haimberger (University of Vienna, Austria) for RICH data. We acknowledge the modeling groups, the PCMDI and WRCP's Working Group on Coupled Modelling (WGCM) for access to CMIP3 multi-model data as well as the Climate Prediction Center (US) for ENSO and QBO index data. J. Fritzer (Wegener Center) is thanked for his efforts in OPS system development and operations. The work was financed by Austrian Science Fund (FWF) grants P18733-N10 and P18837-N10; OPS development also by ESA and the Austrian Research Promotion Agency (FFG-ALR) via projects ProdexCN2 and EOPSCLIM.

References

Baldwin, M. P., M. Dameris, and T. G. Sheperd (2007), How will the stratosphere affect climate change? *Science*, *316*, 1576–1577, doi:10.1126/science.1144303.

Borsche, M., G. Kirchengast, and U. Foelsche (2007), Tropical tropopause climatology as observed with radio occultation measurements from CHAMP compared to ECMWF and NCEP analyses, *Geophys. Res. Lett*., *34*, L03702, doi:10.1029/2006GL027918.

Foelsche, U., G. Kirchengast, A. K. Steiner, L. Kornblueh, E. Manzini, and L. Bengtsson (2008), An observing system simulation experiment for climate monitoring with GNSS radio occultation data: Setup and testbed study, *J. Geophys. Res.*, *113*, D11108, doi:10.1029/2007JD009231.

Foelsche, U., B. Pirscher, M. Borsche, G. Kirchengast, and J. Wickert (2009), Assessing the climate monitoring utility of radio occultation data: From CHAMP to FORMOSAT-3/COSMIC, *Terr. Atmos. Oceanic Sci*., *20*, doi: 10.3319/TAO.2008.01.14.01(F3C).

Haimberger, L., C. Tavolato, and S. Sperka (2008), Towards elimination of the warm bias in historic radiosonde temperature records – some new results from a comprehensive intercomparison of upper air data, *J. Clim*., *21*, 4587–4606, doi:10.1175/2008JCLI1929.1.

Hajj, G. A., et al. (2004), CHAMP and SAC-C atmospheric occultation results and intercomparisons, *J. Geophys. Res.*, *109*, D06109, doi:10.1029/2003JD003909.
Ho, S.-P., et al. (2009), Estimating the uncertainty of using GPS radio occultation data for climate monitoring: Inter-comparison of CHAMP refractivity climate records 2002-2006 from different data centers, *J. Geophys. Res*., doi:10.1029/2009JD011969, in press.
Karl, T. R., S. J. Hassol, C. D. Miller and W. L. Murray (Eds.) (2006), Temperature Trends in the Lower Atmosphere: Steps for Understanding and Reconciling Differences, *A Report by the Climate Change Science Program and the Subcommittee on Global Change Research*, Washington, D. C.
Kursinski, E. R., G. A. Hajj, K. R. Hardy, J. T. Schofield, and R. Linfield (1997), Observing the Earth's atmosphere with radio occultation measurements using the Global Positioning System, *J. Geophys. Res.*, *102*, 23,429–23,465, doi:10.1029/97JD01569.
Leroy, S. S., J. G. Anderson, and J. A. Dykema (2006a), Climate benchmarking using GNSS occultation, in *Atmosphere and Climate: Studies by Occultation Methods*, edited by U. Foelsche, G. Kirchengast, and A. K. Steiner, pp. 287–301, Springer, Berlin.
Leroy, S. S., J. G. Anderson, and J. A. Dykema (2006b), Testing climate models using GPS radio occultation: A sensitivity analysis, *J. Geophys. Res*., *111*, D17105, doi:10.1029/2005JD006145.
Randall, D. A., et al. (2007), Climate models and their evaluation, in *Climate Change 2007: The Physical Science Basis. Contribution of Working Group I to the Fourth Assessment Report of the Intergovernmental Panel on Climate Change*, edited by S. Solomon et al., pp. 589–662, Cambridge Univ. Press, Cambridge, U. K.
Randel, W. J., et al. (2009), An update of observed stratospheric temperature trends, *J. Geophys. Res*., *114*, D02107, doi:10.1029/2008JD010421.
Ringer, M. A., and S. B. Healy (2008), Monitoring twenty-first century climate using GPS radio occultation bending angles, *Geophys. Res. Lett*., *35,* L05708, doi:10.1029/2007GL032462.
Rocken, C., et al. (1997), Analysis and validation of GPS/MET data in the neutral atmosphere, *J. Geophys. Res*., *102*, 29,849–29,866, doi:10.1029/97JD02400.
Santer, B. D., et al. (2008), Consistency of modelled and observed temperature trends in the tropical troposphere, *Int. J. Climatol*., *28*, 1703–1722, doi:10.1002/joc.1756.
Schmidt, T., J.Wickert, G. Beyerle, and S. Heise (2008), Global tropopause height trends estimated from GPS radio occultation data, *Geophys. Res. Lett*., *35*, L11806, doi:10.1029/2008GL034012.
Shindell, D. (2008), Cool ozone, *Nature Geosci*., *1*, 85–86, doi:10.1038/ngeo115.
Steiner, A. K., G. Kirchengast, and H. P. Ladreiter (1999), Inversion, error analysis, and validation of GPS/MET occultation data, *Ann. Geophys*., *17*, 122–138, doi:10.1007/s00585-999-0122-5.
Steiner, A. K., G. Kirchengast, M. Borsche, U. Foelsche, and T. Schoengassner (2007), A multi-year comparison of lower stratospheric temperatures from CHAMP radio occultation data with MSU/AMSU records, *J. Geophys. Res*., *112*, D22110, doi:10.1029/2006JD008283.
Thorne, P. W., D. E. Parker, S. F. B. Tett, P. D. Jones, M. McCarthy, H. Coleman, and P. Brohan (2005), Revisiting radiosonde upper air temperatures from 1958 to 2002, *J. Geophys. Res*., *110*, D18105, doi:10.1029/2004JD005753.
Titchner, H. A., P. W. Thorne, M. P. McCarthy, S. Tett, L. Haimberger, and D. E. Parker (2009), Critically reassessing tropospheric temperature trends from radiosondes using realistic validation experiments, *J. Clim.*, *22*, 465–485, doi:10.1175/2008JCLI2419.1.

Figures:

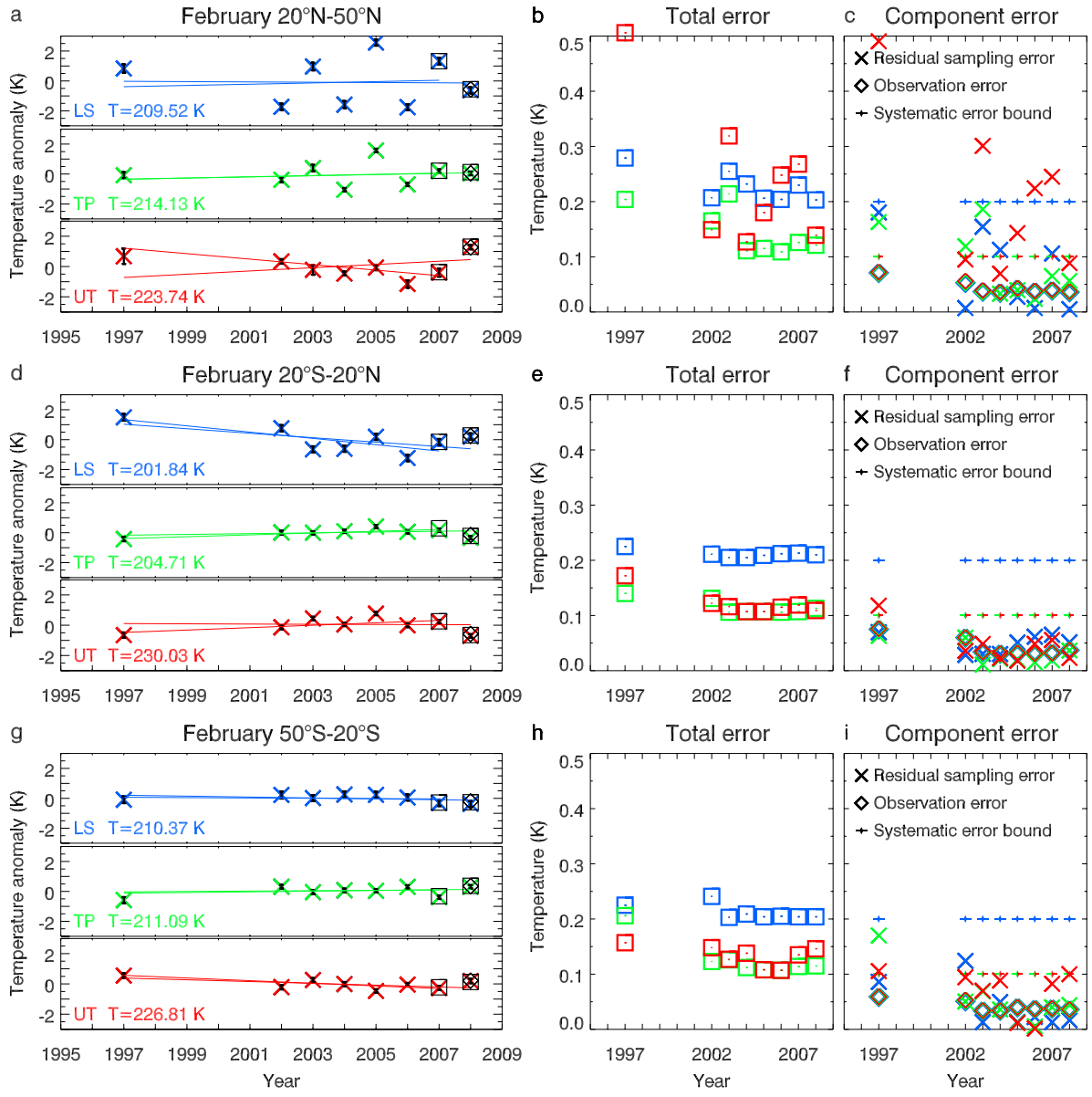

Figure 1. RO temperature anomalies (left panels) and respective errors (right panels) for February 1997–2008, shown for NHE (a–c), tropics (d–f), and SHE (g–i), and for LS (blue), TP (green), and UT (red), respectively. Anomalies (crosses) are referenced to the 1997–2008 mean (values shown) with linear trends fitted (solid line) for 1997–2007 and for 1997–2008. Small error bars (black) denote the respective RO total temperature error for each individual data point. Temperature anomalies for two additional satellites, Formosat-3/COSMIC Flight Model 4 (F3C/FM-4) for February 2007–2008 (black squares) and GRACE for February 2008 (black diamonds), are shown as independent "anchor points" indicating the consistency of RO data. The total error is explicitly shown in b, e, h (squares) and is composed of the residual sampling error (crosses), the observation error (diamonds), and a systematic error bound (c, f, i).

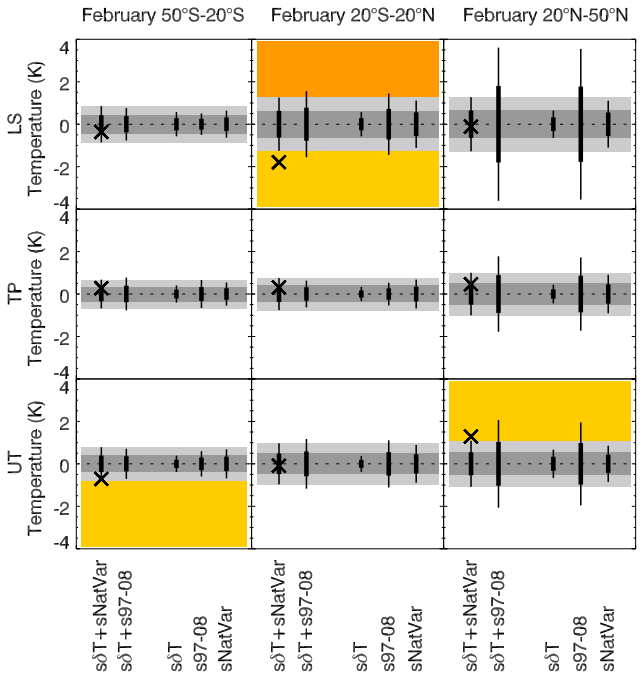

Figure 2. Climate variability, trends, and their significance shown for February 1997–2008 for SHE, tropics, NHE (left to right), and for the LS, TP, UT (top to bottom). RO temperature trends (crosses) are indicated together with the standard error of the trend ($s\delta T$), the standard deviation of the 1997–2008 inter-annual climate variability (s97-08), and the standard deviation of the long-term natural variability of GCM temperature trends (sNatVar). Signal-to-noise ratios are calculated for trend versus 1997–2008 variability ($s\delta T$+s97-08) and for trend versus long-term natural trends variability ($s\delta T$+sNatVar). Signal detection is indicated at the 90 % significance level (yellow) and at the 95 % significance level (orange). A colored bottom part of a sub-panel denotes a significant trend over 1997–2008 variability, a colored top part a significant trend over long-term natural variability. The $s\delta T$+sNatVar standard deviation is shaded in dark gray, twice this standard deviation in light gray.

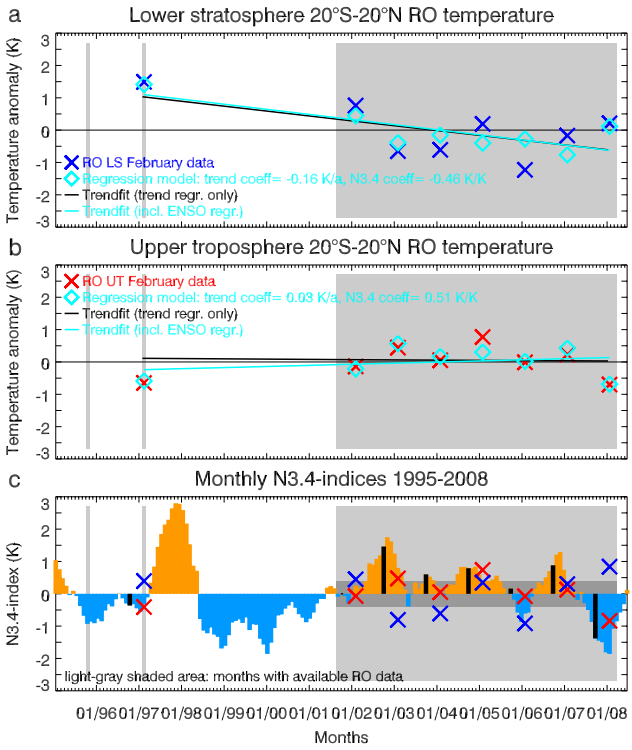

Figure 3. RO temperature anomalies (crosses) and trends (solid lines) accounting for ENSO are shown for February 1997–2008 for the tropical LS (a) and UT (b). Light gray shading indicates periods with RO data availability. Trends were calculated with multiple linear regression (light blue) including monthly N3.4 SST indices (c) with a four month lag (black-highlighted bars). The N3.4 index partly exceeds 0.4 K for El Niño or –0.4 K for La Niña (dark gray). Regression model values are indicated by light blue diamonds. Trends from standard linear regression (Figure 1) are shown in a and b for reference (black) and the crosses in c show the de-trended RO values of a and b for direct comparison.

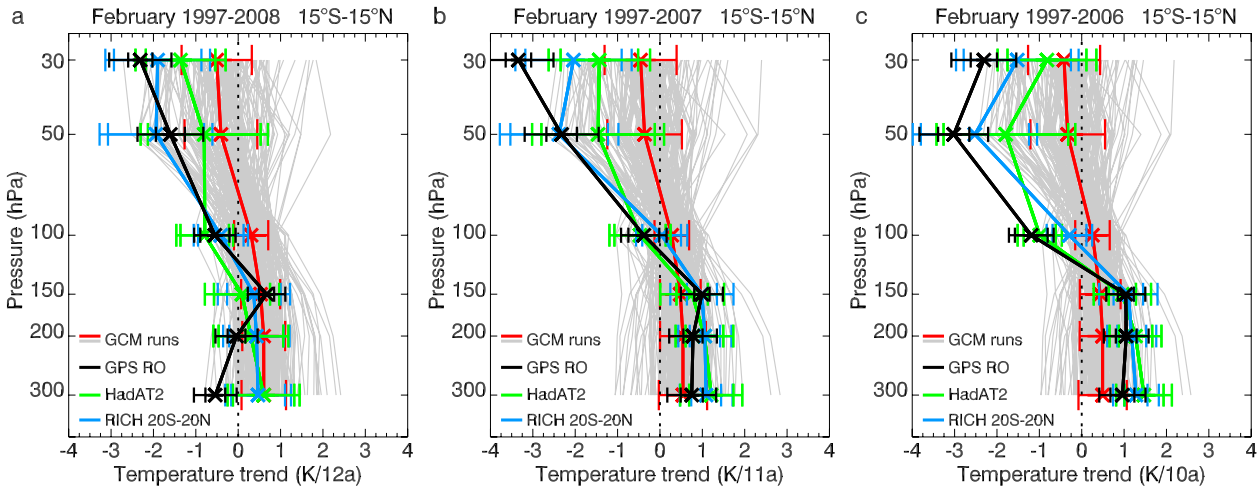

Figure 4. Tropical (15°S–15°N) temperature profile trends at 6 pressure levels from 300–30 hPa shown for February 1997–2008 (a), 1997–2007 (b), and 1997–2006 (c). RO data (black) are compared to HadAT2 (green) and RICH (blue) radiosonde data, and to the mean (red) and individual 10–12 year trends (gray) of a multi-model multiple realizations data set of IPCC AR4 climate model runs (see auxiliary material) within 2001–2020. Model error bars denote one standard deviation of the trends ensemble, and data error bars denote the error of the trend (inner bar) plus natural variability (wider bar).

Auxiliary Material for Paper 2009GL039777

Atmospheric temperature change detection with GPS radio occultation 1995 to 2008

A. K. Steiner, G. Kirchengast, B. C. Lackner, B. Pirscher, M. Borsche, U. Foelsche
Wegener Center for Climate and Global Change (WegCenter) and Institute for Geophysics, Astrophysics, and Meteorology (IGAM), University of Graz, Leechgasse 25, A-8010 Graz, Austria
e-mail: andi.steiner@uni-graz.at; gottfried.kirchengast@uni-graz.at

This auxiliary material contains a methods summary, a detailed description of data, processing, and computation methods as well as 9 figures (Figures S1 to S9), 3 tables (Tables S1 to S3), and auxiliary references.

Auxiliary Methods Summary

GPS RO sounding. The GPS dual-frequency radio signals are refracted and retarded by the atmospheric density field during their propagation to a receiver on a Low Earth Orbit (LEO) satellite. An occultation event occurs whenever a GPS satellite sets behind (or rises from) the horizon and its signals are occulted by the Earth's limb as viewed from the receiver. Vertical scanning is provided by the relative motion of the GPS and LEO satellites. The signal disturbance is exploited to gain information on the atmospheric thermal structure from phase delay measurements and orbit information based on precise timing with atomic clocks.

RO retrieval and errors. RO atmospheric profiles were retrieved with Wegener Center's Occultation Processing System OPSv5.4 (Table S3) based on RO phase delay and orbit data of the University Corporation for Atmospheric Research, Boulder, CO, USA. Regarding retrieval errors, residual errors from the GPS dual-frequency ionospheric correction and the background information-dependent initialization of profiles at high altitudes are of climatological interest. Residual ionospheric errors were estimated to induce a temperature bias of 0.1–0.2 K at 20–25 km for solar maximum versus minimum conditions [*Gobiet and Kirchengast*, 2004; *Rocken et al*., 2009] (Figure S8), which becomes negligible in > 10-year temperature trends below 25 km height (< 0.04 K/decade). Temperature biases due to initialization were found < 0.1–0.2 K below 30 km height for non-polar (< 60° latitude) large-scale means as used in this study [*Gobiet and Kirchengast*, 2004; *Gobiet et al*., 2007; *Steiner et al*., 2009]; and long-term variation of these is expected smaller [*Steiner et al*., 2009; ref. main paper: *Steiner et al*., 2007; *Ho et al*., 2009]. Furthermore, we derived temperature profiles assuming dry air conditions ("dry temperature"), which is closely valid in the UTLS down to about 8 km [*Steiner et al*., 2009]. While negligible in the LS, the moisture effect gains importance in the tropical UT as estimated from ECMWF analyses (Figure S9); in the 300–200 hPa layer (~9–12 km) it results in a slightly larger warming trend in actual temperature than in dry temperature, with a difference of ~0.07 K/decade, implying that RO dry temperature trends slightly underestimate actual UT warming trends.

RO climatologies and errors. We computed monthly mean atmospheric fields through sampling and averaging of RO profiles (see auxiliary data and methods) by which accurate 10°-zonal mean RO climatologies can be obtained already for single LEO RO satellites like GPS/Met and CHAMP with well defined error characteristics [*Gobiet et al*., 2007; *Pirscher et al.,* 2007; *Foelsche et al.*, 2008a; ref. main paper: *Foelsche et al.* 2009]. The sampling error due to uneven and sparse sampling in space and time is <0.3 K in the UTLS, with the local time component

error <0.15 K [*Pirscher et al.*, 2007], and can be estimated and subtracted [*Pirscher et al.*, 2007; ref. main paper: *Foelsche et al*., 2009; *Ho et al*., 2009]. Residual sampling errors are very small (<0.1 K vertically resolved and <0.03 K for UTLS means in large-scale areas) as found by *Foelsche et al*. [2008b, 2009]. The statistical observational error becomes negligible in climatologies (<0.01–0.1 K) due to the averaging over hundreds of profiles per zonal band. Overall the total error is estimated to <0.3–0.5 K below 30 km [*Foelsche et al*., 2008a]. Structural uncertainties amongst climatologies of different RO processing centers, including Wegener Center, are low with <0.03 %/5a for refractivity trends in large-scale means and <0.06 K/5a for temperature trends as found for current data sets [ref. main paper: *Ho et al*., 2009].

Detection study. Building on these favorable error characteristics, we focus our trend detection study on the UTLS between 300–30 hPa (~9–25 km), where the data quality is optimal, and on 50°N–50°S. High latitudes are not examined due to known biases in background stratospheric temperatures used for the GPS/Met data initialization (ERA-40 reanalysis) (see auxiliary data and methods) and frequently higher RO sampling errors there [*Steiner et al*., 2009]. We performed the analysis for three large-scale zonal means: tropics 20°S–20°N, Northern Hemisphere extratropics 20°N–50°N (NHE), Southern Hemisphere extratropics 20°S–50°S (SHE), and for three vertical layer means: upper troposphere 300–200 hPa (UT), tropopause region 200–100 hPa (TP), and lower stratosphere 100–30 hPa (LS), the layer terms referring to the tropics. After subtraction of the estimated sampling error from the monthly mean zonal climatologies, a standard linear regression analysis was performed based on temperature anomalies for February (8 years of data out of 12 years) and October (8 years of data out of 13 years), respectively, as well as multiple linear regression focusing on the tropics; trend significance was determined with a Students *t*-test (see auxiliary data and methods).

Auxiliary Data and Methods

Radio Occultation (RO) Data

First RO observations of the Earth's atmosphere are available from the GPS/Met proof-of-concept mission intermittently within the years 1995–1997 [*Ware et al*., 1996; *Kursinski et al*., 1996]. Essentially continuous RO observations are provided by the German CHAMP mission [*Wickert et al*., 2004] establishing the first multi-year RO climate record [*Gobiet et al*., 2005; ref. main paper: *Borsche et al*., 2007; *Schmidt et al*., 2008] covering seven years until September 2008. The only data gap in July/August 2006 can be filled with RO data from the GRACE (Gravity and Climate Experiment) satellite [*Wickert et al*., 2005]. RO atmospheric profiles from the Argentine SAC-C (Satelite de Aplicaciones Cientificas-C) satellite [*Hajj et al*., 2004] are available within 2001–2002. Formosat-3/COSMIC (F3C, Taiwan/US), a 6 satellites RO mission [*Rocken et al*., 2000; *Wu et al*., 2005], and the European MetOp mission [*Luntama et al*., 2008] started in 2006. The latter will operationally provide high-quality RO observations until the year 2020 [*Luntama et al*., 2008]. Also the German TerraSAR-X satellite, launched in 2007, provides RO data [*Wickert et al*., 2009].

For this study we used GPS/Met and CHAMP data, where the CHAMP data have been, in overlapping periods, inter-validated with F3C data and SAC-C data. In this context we also used available RO data from two satellites as independent "anchor points", i.e. F3C/FM-4 (F3C/Flight Model 4) for February 2007–2008 and GRACE for February 2008. The agreement in the 9–

25 km range is very good with a difference of generally < 0.1 K in large-scale monthly means [*Foelsche et al*., 2008b; 2009]. On RO data on-line availability see [*Foelsche et al*., 2008a] and "Processing of RO Profile Data" below.

Radiosonde Data

Radiosonde data from the Hadley Centre/MetOffice, UK, (HadAT2) are available at www.hadobs.org [ref. main paper: *Thorne et al.,* 2005; *Titchner et al*., 2009]. The resolution is 10 degrees in longitude by 5 degrees in latitude at 9 pressure levels (850 hPa, 700 hPa, 500 hPa, 300 hPa, 200 hPa, 150 hPa, 100 hPa, 50 hPa, 30 hPa).

Newly homogenized records from the University of Vienna, Austria, (RICH) are available at ftp://srvx6.img.univie.ac.at/pub/rich_gridded.nc [ref. main paper: *Haimberger et al*., 2008]. The resolution is 10 degrees in latitude by 10 degrees in longitude at 12 pressure levels (850 hPa, 700 hPa, 500 hPa, 400 hPa, 300 hPa, 250 hPa, 200 hPa, 150 hPa, 100 hPa, 70 hPa, 50 hPa, 30 hPa).

We used the data at the 6 pressure levels 300 hPa, 200 hPa, 150 hPa, 100 hPa, 50 hPa, 30 hPa.

We note that station coverage in the tropical Pacific region (90°W–180°W) is very sparse, with no radiosonde stations in the 5°N–5°S ENSO core region and only very few within 15°N–15°S (for HadAT2 coverage see Figure 7 of [ref. main paper: *Thorne et al.,* 2005], for RAOBCORE/RICH see Figure 1 of [ref. main paper: *Haimberger et al*., 2008] and the station record at http://homepage.univie.ac.at/leopold.haimberger/RAOBCORE_T_1.4.html).

Global Climate Model Data

We used a multi-model multiple-realizations data set of three selected representative GCMs of the IPCC AR4 models [*Cordero and de Forster*, 2006; *IPCC*, 2007]:

- Community Climate System Model (CCSM3) of the National Centers for Environmental Prediction (NCEP) and the National Center for Atmospheric Research (NCAR), USA [*Collins et al*., 2006].
- ECHAM5 of the Max-Planck-Institute for Meteorology Hamburg (MPI) [*Roeckner et al*., 2003],
- HadCM3 of the Hadley Centre for Climate Prediction and Research of the UK-MetOffice (Hadley Centre/MetOffice (UKMO)) [*Pope et al*., 2000; *Gordon et al*., 2000].

Table S1 gives an overview on resolution, time-range, and number of runs. Pre-industrial control (PreInCtl) runs are used for the calculation of long-term variability of trends over the 10–13-year periods of interest (Figure S2). We estimated natural variability by sampling trends over time periods of the length of the respective RO time periods. In addition we checked sensitivities by using an intermittency mask for years exactly matching RO data as well as by removing or not removing ENSO influenced years, which all led to minor differences in the results for the large-scale domains we have chosen. The models exhibit different characteristics of internal variability (Figure S2). ECHAM5 shows stronger variation than CCSM3 while HadCM3 lies in between [*Meehl et al*., 2007; ref. main paper: *Leroy et al*., 2006b]. Overall they cover a representative range of variability as stated by the IPCC AR4 [*IPCC*, 2007, page 686]: "*There is no evidence that the variability in paleoclimatic reconstructions that is not explained by forcings is stronger than that in models and simulations of the last 1 kyr*."

For trend comparison (Figure 4) we use forced runs of Special Report on Emission Scenarios (SRES) A2 and B1 with prescribed greenhouse gas forcing, sampling trends from the time period 2001–2020 using an intermittency mask consistent with RO data. All selected models use ozone depletion and recovery forcings in their simulations [*Roeckner et al*., 2007], which play an

essential role for simulating stratospheric temperatures [ref. main paper: *Shindell*, 2008]. The three selected models comprise a representative set of GCMs with respect to the whole set of IPCC AR4 models [*IPCC*, 2007, Figure 10.5; *Reichler and Kim*, 2008].

The data are available from the World Climate Research Programme's Working Group on Coupled Modelling (WCRP's WGCM) multi-model database via the Program for Climate Model Diagnostics and Intercomparison (PCMDI) at Lawrence Livermore National Laboratory (USA) at http://www-pcmdi.llnl.gov/ipcc/about_ipcc.php.

Processing of RO Profile Data

At the Wegener Center we developed an Occultation Processing System (OPS) for best possible exploitation of RO data for climate research with focus on minimizing the influence of ionospheric residuals and of background information in the retrieval. RO atmospheric profiles for this study were retrieved with version OPSv5.4 (Table S3) [*Borsche et al*., 2006; *Kirchengast et al.*, 2007; *Borsche*, 2008; *Foelsche et al*., 2008a; ref. main paper: *Foelsche et al*., 2009; *Ho et al*., 2009] based on RO phase delay and orbit data from the University Corporation of Atmospheric Research/COSMIC Data Analysis and Archive Center (UCAR/CDAAC), Boulder, CO, USA (version 2005.1720 for GPS/Met data, versions 2007.1200 until May 2007, 2007.1700 in June/July 2007, 2007.3200 since August 2007 for CHAMP data, and version 2007.3200 for GRACE and F3C/FM-4 data).

Previous Wegener Center processing system versions (OPSv5.3 [ref. main paper: *Ho et al*., 2009]; OPSv5.2 [ref. main paper: *Foelsche et al*., 2009]; CCRv2.3 [*Gobiet et al.*, 2007; *Foelsche et al*., 2008a; *Steiner et al.*, 2009; ref. main paper: *Borsche et al.*, 2007] that used phase delay and orbit data from the German Research Centre for Geoscience (GFZ) Potsdam, Germany, have closely the same characteristics as OPSv5.4 and as for trend analysis they lead to the same main results as presented in this paper. This was found from cross-testing with previous OPS versions using phase and orbit data from different data centers and is also confirmed by the findings of [ref. main paper: *Ho et al*., 2009], showing low structural uncertainty among monthly mean climatological results of different RO processing centers.

An overview on the major processing steps of Wegener Center's OPSv5.4 is given in Table S3. Briefly, first the time derivation of phase delay profiles yields Doppler shifts from which bending angles are derived using precise orbit information. The contribution of the ionosphere is removed by linear combination of bending angles at two frequencies. Background information is included only at the stage of bending angle initialization with statistical optimization at high altitudes [*Gobiet and Kirchengast*, 2004]. Bending angles from ECMWF short-range forecasts are generally used as background. For GPS/Met we used ERA-40 reanalysis data, due to the inadequate height range and resolution of ECMWF forecasts at that time (sensitivity checks verified that retrieval results below 25 km height do not significantly depend on the choice of background, as long as it is reasonably adequate, consistent with literature [e.g., *Gobiet and Kirchengast*, 2004; *Gobiet et al*., 2007; ref. main paper: *Kursinski et al*., 1997]). The statistical optimization stabilizes the retrieval in the upper stratosphere and mesosphere and also contributes to minimize residual ionospheric errors, which depend on solar variability [*Gobiet and Kirchengast*, 2004]. Bending angles are further inverted to refractivity (equivalent to air density), which is integrated to yield pressure profiles and, in turn, (dry) temperature profiles are obtained via the equation of state.

The Wegener Center OPSv5.4 data are available on-line via www.wegcenter.at/globclim.

Computation of Basic RO Climatologies

Monthly mean zonal mean climatologies were obtained by "binning and averaging" [*Borsche et al*., 2006; *Foelsche et al*., 2008a] of the retrieved temperature profiles. For this study, the basic resolution was zonal bins of 5° latitudinal width (i.e., 36 bins) at an MSL (mean-sea-level) altitude grid with regular 200 m spacing. For each month all RO profiles in a bin were sampled and averaged, weighted by the cosine of the latitude. The mean temperature profile $\overline{T(z)}$ in each bin is given by

$$\overline{T(z)} = \frac{1}{\sum_{i=1}^{n_{\mathrm{prof}}(z)} \cos(\varphi_i)} \sum_{i=1}^{n_{\mathrm{prof}}(z)} T_i(z,\varphi_i)\cos(\varphi_i)\,, \tag{1}$$

where n_{prof} is the number of profiles in each bin. Together with the climatologies the sampling error is estimated through use of ECMWF analysis fields, which are assumed to approximately represent the "true" variability of the atmosphere (a good assumption for the purpose, see [*Foelsche et al*., 2008b; 2009]). A detailed description of the setup of RO based climatologies and estimation of errors is given in [*Foelsche et al*., 2008a]. Also these climatology data are available, at 10°-latitudinal resolution, via www.wegcenter.at/globclim.

Computation of Zonal Means and Layer Means

Weighted averages of larger-scale zonal means, as used for this study, were produced by weighting with the cosine of the respective 5°-latitude bands; consistently for all data sets.
Vertical layer means for RO were calculated by using all available levels n_{lev} within a defined layer and by weighting with the layer thickness. Since RO temperatures and RO pressures are available at the same MSL altitude grid z, the altitude levels falling into the respective pressure layer (n_{lev} levels) were determined and vertical temperature layer means, $\overline{T}_{\mathrm{layer}}$, calculated as

$$\overline{T}_{\mathrm{layer}} = \frac{\frac{1}{2}\sum_{i\mathrm{lev}=1}^{n\mathrm{lev}-1}\left(z_{i\mathrm{lev}+1} - z_{i\mathrm{lev}}\right)\cdot\left(T_{i\mathrm{lev}} + T_{i\mathrm{lev}+1}\right)}{\sum_{i\mathrm{lev}=1}^{n\mathrm{lev}-1}\left(z_{i\mathrm{lev}+1} - z_{i\mathrm{lev}}\right)}\,. \tag{2}$$

For trend comparison with other data sets RO temperature as function of pressure was interpolated to the respective pressure levels used in this study (linearly on log-pressure coordinate). Radiosonde and IPCC AR4 GCM data were available at the chosen common pressure levels 300 hPa, 200 hPa, 150 hPa, 100 hPa, 50 hPa, 30 hPa.

Computation of Trends with Standard Linear Regression

Standard linear regression for trend evaluation was performed for monthly mean zonal mean temperature climatologies for the months of February 1997–2008 and October 1995–2007, respectively. Trends b were calculated by considering the individual errors for each month, consisting of the residual sampling error s_{samp} (50 % of the sampling error), a systematic error bound s_{sys} of 0.2 K above 100 hPa and of 0.1 K below, and the observation error, s_{obs},

$$s_{\mathrm{obs}} = \frac{1\ \mathrm{K}}{\sqrt{n_{\mathrm{prof}}}}\,, \tag{3}$$

with n_{prof} as the number of RO profiles in the considered domains (Table S2). The total error s is then obtained by

$$s = \sqrt{\left(s_{\mathrm{samp}}\right)^2 + \left(s_{\mathrm{sys}}\right)^2 + \left(s_{\mathrm{obs}}\right)^2} \; . \tag{4}$$

Linear least-squares fitting [*Press et al*., 1987] of a straight line $y(t) = a + bt$ to n data points y as function of time t is performed with the requirement of χ^2 to be a minimum,

$$\chi^2(a,b) = \sum_{i=1}^{n} \left[\frac{y_i - \left(a + bt_i\right)}{s_i} \right]^2 \stackrel{!}{=} \mathrm{Min} \; . \tag{5}$$

The fit parameters a and b are calculated as

$$a = \frac{\sum \frac{t_i y_i}{s_i^2} - b \sum \frac{t_i^2}{s_i^2}}{\sum \frac{t_i}{s_i^2}}, \qquad b = \frac{\sum \frac{1}{s_i^2} \sum \frac{t_i y_i}{s_i^2} - \sum \frac{t_i}{s_i^2} \sum \frac{y_i}{s_i^2}}{\sum \frac{1}{s_i^2} \sum \frac{t_i^2}{s_i^2} - \left(\sum \frac{t_i}{s_i^2} \right)^2} \; . \tag{6}$$

The error of the trend s_b is obtained by

$$s_b^2 = \frac{\sum \frac{1}{s_i^2}}{\sum \frac{1}{s_i^2} \sum \frac{t_i^2}{s_i^2} - \left(\sum \frac{t_i}{s_i^2} \right)^2} \; . \tag{7}$$

The temperature trend δT for the total investigated time period n_{years} is given by $\delta T = b \, n_{\mathrm{years}}$, together with the error of the trend, $s_{\delta T} = \sqrt{s_b^2} \, n_{\mathrm{years}}$.

Inter-annual variability is represented by the de-trended standard deviation,

$$s_{97-08} = \sqrt{\frac{1}{n-m} \sum_{i=1}^{n} \left(y_i - a - bt_i \right)^2} \; , \tag{8}$$

with m as the number of fitted parameters. Long-term natural variability of trends, s_{NatVar}, was calculated based on preindustrial control runs as described in Section "Global Climate Model Data" above. The mean variability of the control runs (Table S1) of three GCMs, s_{gcm}, was used,

$$s_{\mathrm{NatVar}} = \frac{1}{n_{\mathrm{gcm}}} \sum_{i=1}^{n_{\mathrm{gcm}}} s_{\mathrm{gcm}_i} \; , \tag{9}$$

with n_{gcm} being the number of model runs. The signal-to-noise ratio (SNR) was calculated with respect to inter-annual climate variability and with respect to long-term natural variability of climate trends,

$$\mathrm{SNR}_{(s_{\delta T} + s_{97-08})} = \frac{\delta T}{\sqrt{s_{\delta T}^2 + s_{97-08}^2}}, \quad \mathrm{SNR}_{(s_{\delta T} + s_{\mathrm{NatVar}})} = \frac{\delta T}{\sqrt{s_{\delta T}^2 + s_{\mathrm{NatVar}}^2}} \; . \tag{10}$$

The trend's significance was tested with a Students t-test. A trend for the period February 1997–2007 (October 1995–2006) with 7 years of data is considered significant at the respective significance level if the SNR exceeds the t-test values for 5 degrees of freedom (90 % significance level: $2.015 < \mathrm{SNR} < 2.570$; 95 % significance level: $2.570 < \mathrm{SNR} < 4.032$). A trend

for the period February 1997–2008 (October 1995–2007) with 8 years of data is considered significant at the respective significance level if the SNR exceeds the *t*-test values for 6 degrees of freedom (90 % significance level: $1.940 < \mathrm{SNR} < 2.447$; 95 % significance level: $2.447 < \mathrm{SNR} < 3.707$).

Regarding SNR in the tropics, we note here the results of a refined layer definition of the tropical LS (70–30 hPa instead of 100–30 hPa, i.e., staying a bit apart from the tropopause). This yielded somewhat larger trends (within the standard deviation of the 100–30 hPa trends) but also larger variability due to a smaller vertical averaging domain. Overall the tropical SNR was slightly further increased but with statistical significances remaining unchanged.

We also checked auto-correlation of the temperature time series, which influences trend detection (times), besides natural variability and measurement uncertainty [*Weatherhead et al*., 1998; 2002; *Leroy et al*., 2008]. HadAT2 radiosonde data from 1958–2007 and RO data from 2001–2008 were investigated for this check. Auto-correlation was found negligible for the one-month-per-year time series of RO and radiosonde data as used in this study (while continuous monthly-mean and annual-mean data clearly show auto-correlation as we also co-checked in respective sensitivity tests). Thus no correlation was used in this study in the statistical testing.

Computation of Trends with Multiple Linear Regression

Multiple linear regression [*Von Storch und Zwiers*, 1999] was used to compute trends while also including ENSO and QBO signals, and taking into account the individual error for each month,

$$y(t) = a_0 + a_1 t + a_2 \mathrm{N3.4}(t) \left(+ a_3 \mathrm{QBO}(t)\right) + \varepsilon \,, \qquad (11)$$

where the regression coefficients comprise a constant a_0, the trend coefficient a_1, the N3.4 coefficient a_2, and the QBO coefficient a_3, and a residual error term ε.

ENSO was represented by the monthly Nino 3.4 (N3.4) Sea Surface Temperature (SST) index. N3.4 is the average sea surface temperature anomaly in the region 5°N–5°S and 170°W–120°W with respect to the base period 1961–1990. An El Niño or La Niña event is identified if the 5-month running-average of the N3.4 index exceeds +0.4 K for El Niño or –0.4 K for La Niña for at least 6 consecutive months.

QBO is represented by the monthly QBO index of zonally averaged winds at 50 hPa over the equator. From correlation analysis of RO data at study resolution we found a maximum correlation between ENSO and RO temperature at a lag of 4 months (temperature lagging ENSO) comparable to the results of *Angell* [2000]. Maximum correlation between QBO and RO temperature was found at a lag of 3 months (temperature lagging QBO), which is consistent with the findings of *Seidel et al.* [2004]. We thus used these lag estimations in the multiple linear regression. Co-estimating both QBO and ENSO in the LS over-fitted the data (Figure S5; N3.4 coefficient of –1.10 K/K) but QBO showed no important influence (QBO coefficient of 0.07 K/m/s). We thus finally co-estimated an ENSO signal only (Figure 3).

N3.4 and QBO indices are provided by the U.S. Climate Prediction Center (CPC) and available on-line at www.cpc.ncep.noaa.gov/data/indices/.

Auxiliary Figures:

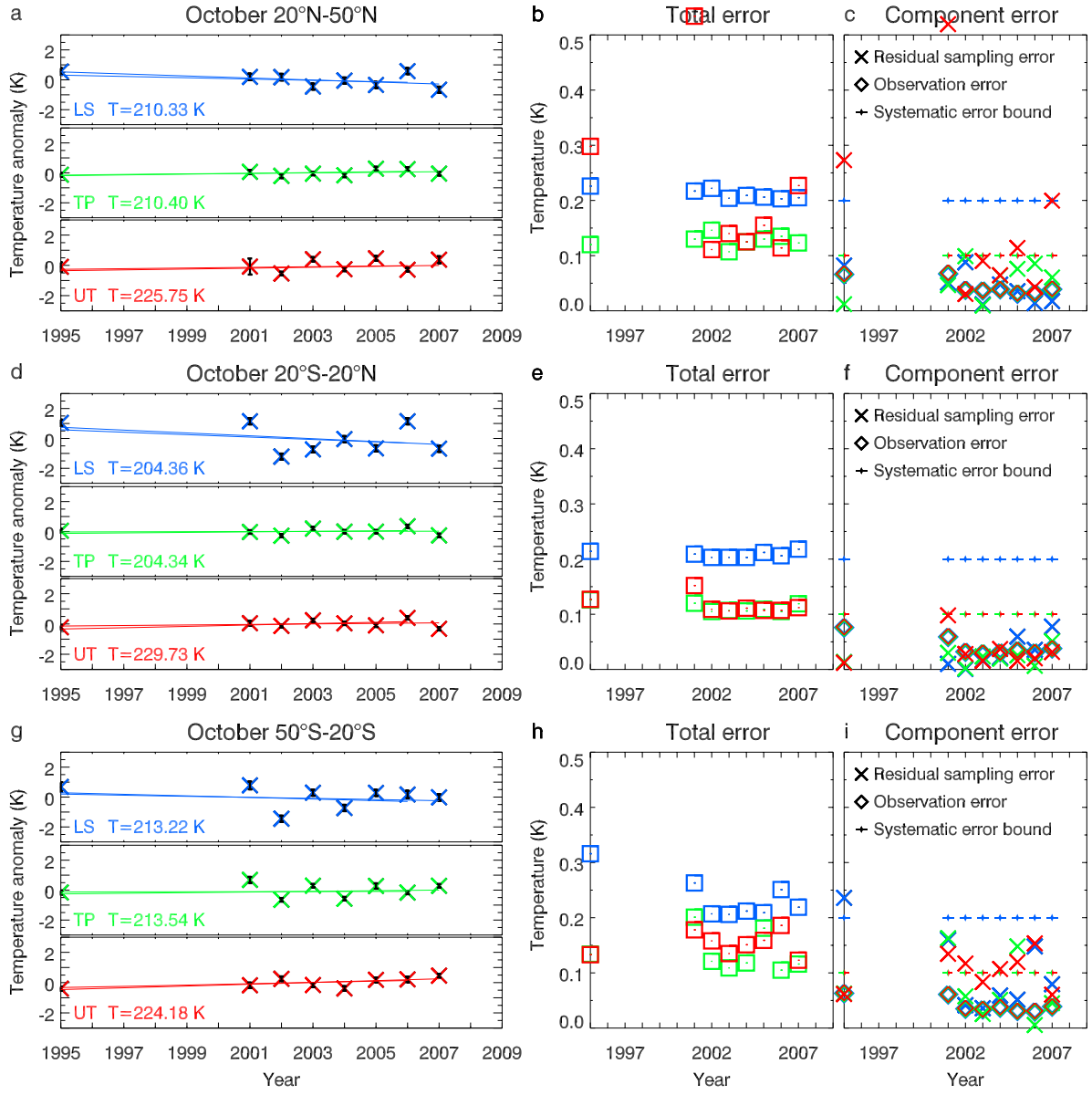

Figure S1: RO temperature anomalies (left panels) and respective errors (right panels) for October 1995–2007, shown for NHE (**a–c**), tropics (**d–f**), and SHE (**g–i**), and for LS (blue), TP (green), and UT (red). Anomalies (crosses) are referenced to the 1995–2007 mean (values shown) with linear **trends** fitted (solid line) for 1995–2006 and for 1995–2007. Error bars (black) denote the respective RO total temperature error for each individual month. This total error is explicitly shown in **b**, **e**, **h** (squares) and is composed of residual sampling error (crosses), observation error (diamonds), and a systematic error bound (**c**, **f**, **i**).

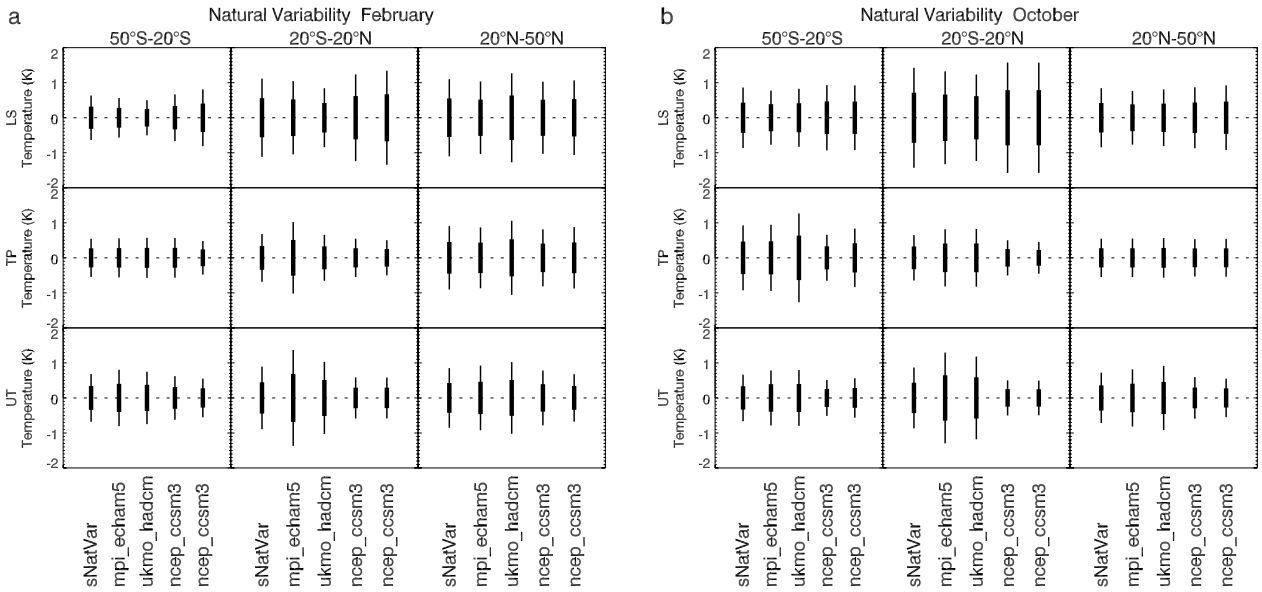

Figure S2: Natural climate variability of temperature trends for February (**a**) and October (**b**) shown for SHE, the tropics, NHE (left to right) and for the layers LS, TP, UT (top to bottom) as estimated from preindustrial control runs of three representative IPCC AR4 GCMs (Table S1): MPI/ECHAM5, UKMO/HadCM3, and NCEP/CCSM3 (2 runs). The mean of all runs (*s*NatVar) is used to represent the best-estimate long-term natural climate variability for signal detection (see also Auxiliary Data and Methods, section Global Climate Model Data).

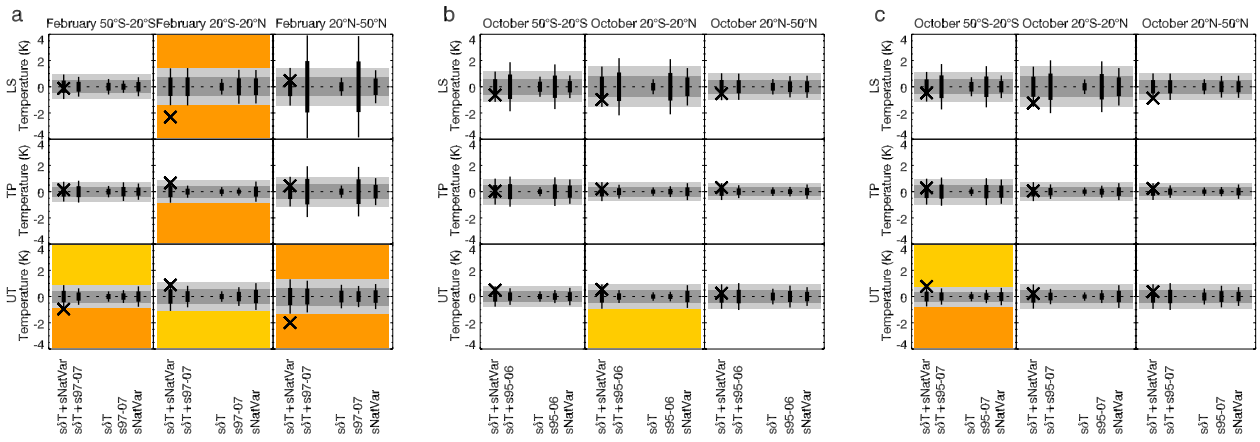

Figure S3: Climate variability, trends, and their significances for February 1997–2007 (**a**), October 1995–2006 (**b**), October 1995–2007 (**c**) are shown for SHE, tropics, NHE (left to right) and for the LS, TP, UT (top to bottom). RO temperature trends (crosses) are indicated together with the standard error of the trend ($s\delta T$), the standard deviation of the inter-annual climate variability (s97-07; s95-06; s95-07), and the standard deviation of the long-term natural variability of GCM temperature trends (sNatVar). Signal-to-noise ratios are calculated for trend versus, e.g., 1997–2007 variability ($s\delta T$+s97-07) and for trend versus long-term natural trends variability ($s\delta T$+sNatVar). Signal detection is indicated at the 90 % significance level (yellow) and at the 95 % significance level (orange). A colored bottom part of a sub-panel denotes a significant trend over 1997–2008 variability, a colored top part a significant trend over long-term natural variability. The $s\delta T$+sNatVar standard deviation is shaded in dark gray, twice this standard deviation in light gray.

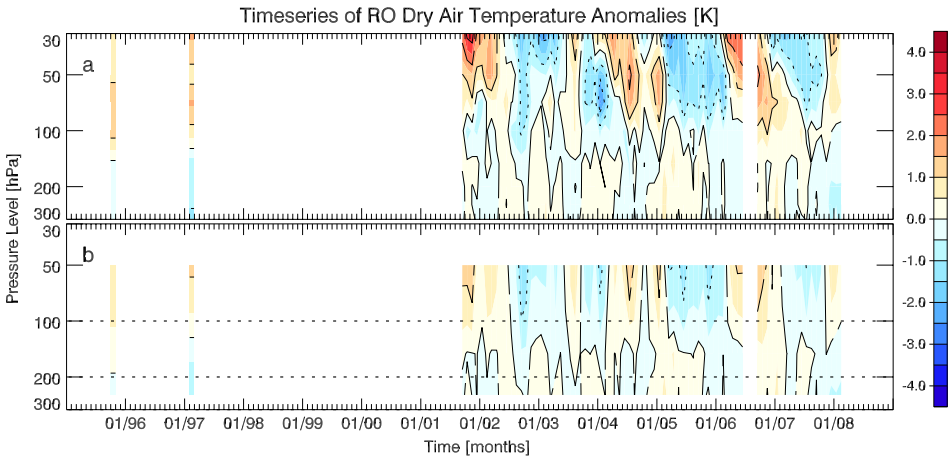

Figure S4: The Quasi-Biennial Oscillation (QBO) pattern in RO CHAMP temperature anomalies is clearly observed in the tropical LS between 15°N–15°S (**a**) [*Randel et al*., 2003; *Schmidt et al*., 2004] but becomes very small when averaging over the larger domain of 20°S–20°N and 100–30 hPa (**b**).

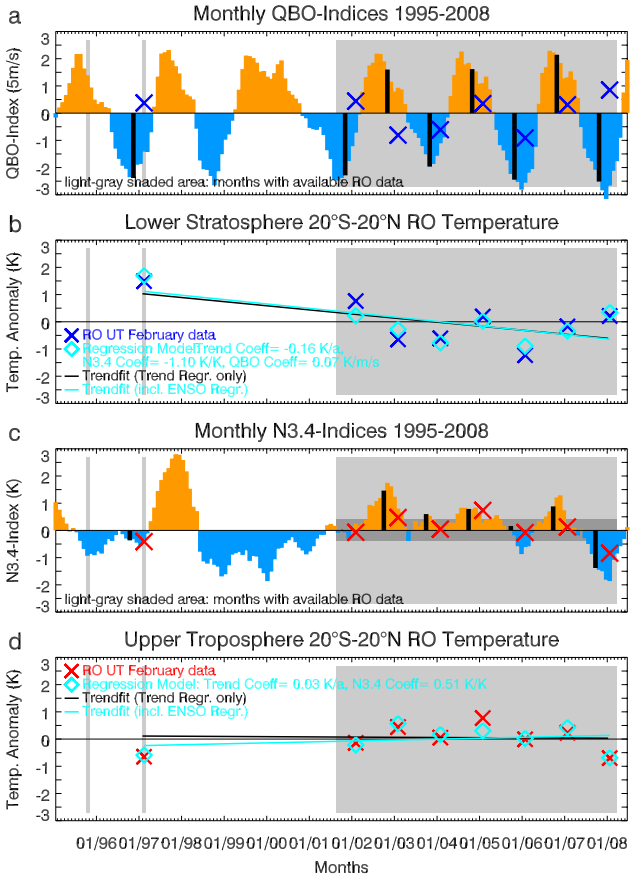

Figure S5: Multiple linear regression of RO temperature anomalies including monthly QBO indices of 50 hPa winds with a three month lag (black-highlighted bars) in the LS (**a**) and including the monthly N3.4 SST indices with a four month lag (black-highlighted bars) in UT and LS (**c**). RO temperature anomalies (crosses) and trends (solid light blue) are shown for February 1997–2008 for the tropical LS (**b**) and the tropical UT (**d**). Light gray shading indicates RO data availability. Regression model values are indicated by light blue diamonds in **b** and **d**, and trends from standard linear regression are shown for reference (black). The crosses in **a** and **c** show the de-trended RO values of the LS (**b**) and the UT (**d**) for direct comparison. Co-estimating both QBO and ENSO in the LS over-fitted the data (N3.4 coefficient of –1.10 K/K) but QBO showed no important influence (QBO coefficient of 0.07 K/(m/s)).

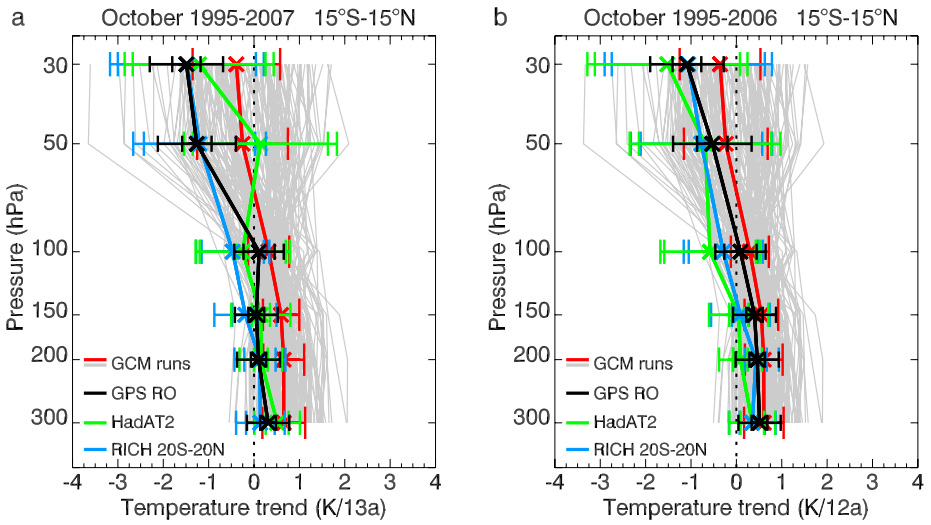

Figure S6: Tropical (15°S–15°N) temperature profile trends at 6 pressure levels from 300–30 hPa shown for October 1995–2007 (**a**) and for October 1995–2006 (**b**). RO data (black) are compared to HadAT2 (green) and RICH (blue) radiosonde data, and to the mean (red) and individual 12–13 year trends (gray) of a multi-model multiple realizations data set of IPCC AR4 climate model runs (see auxiliary data and methods) within 2001–2020. Model error bars denote one standard deviation of the trends ensemble, and data error bars denote the error of the trend (inner bar) plus natural variability (wider bar).

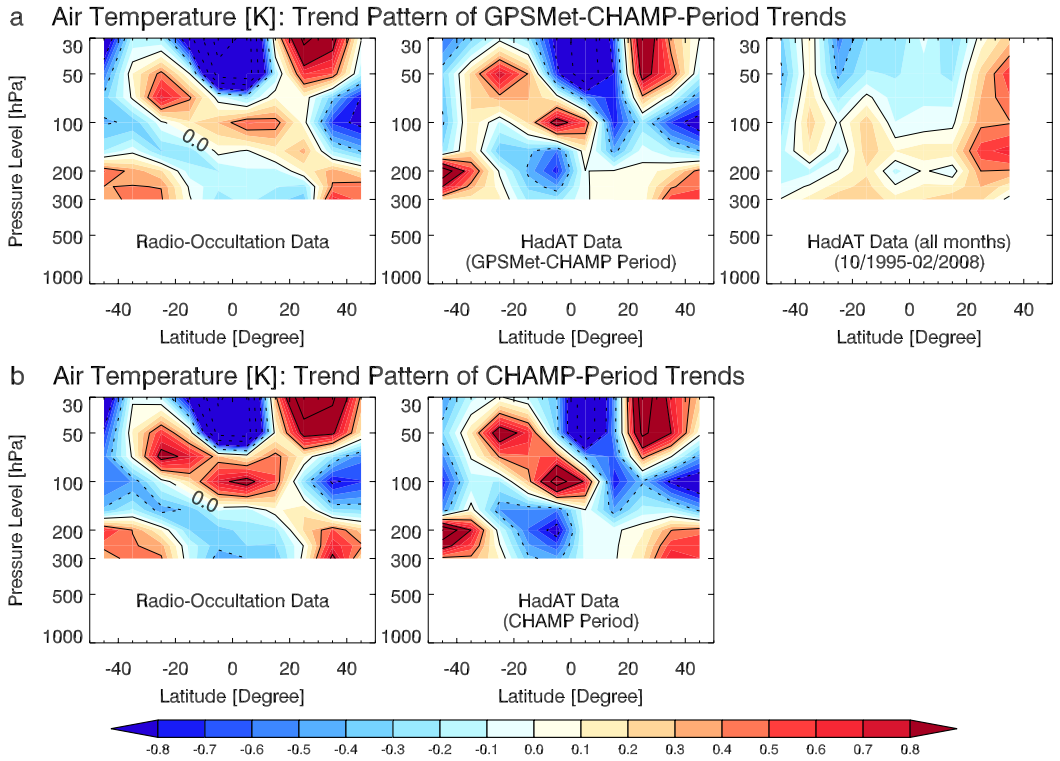

Figure S7: Trend pattern (temperature change over the time period considered) of RO monthly mean temperature anomalies at 10° zonal resolution (left) compared to corresponding HadAT2 radiosonde temperature anomalies (middle) for the GPS/Met plus CHAMP period (1995, 1997, 2001–2008) (**a**) and for the CHAMP period only (2001–2008) (**b**). Also shown, for context, is the trend pattern of HadAT2 radiosonde temperatures for the continuous period 1995–2008 (**a**, right).

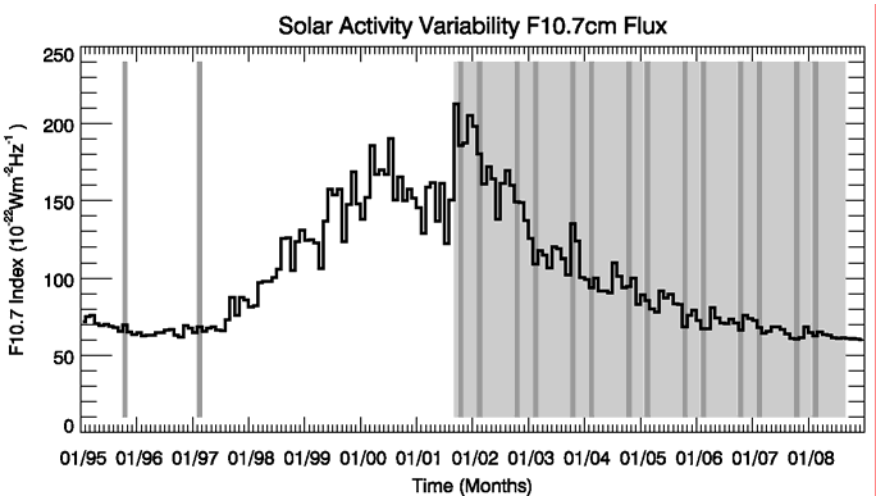

Figure S8: Variability of solar activity represented by the monthly-mean solar flux at 10.7 cm wavelength. The F10.7 index is given in solar flux units (1 sfu = 10^{-22} $Wm^{-2}Hz^{-1}$). Indicated are months with RO data availability (gray) and the specific months of February and October used in this study (dark gray). The February (October) values range from 62.5 (60.4) at low solar activity to 180.1 (185.9) near high solar activity. F10.7 data are available from the National Geophysical Data Center at ftp://ftp.ngdc.noaa.gov/STP/SOLAR_DATA/SOLAR_RADIO/FLUX/MONTHPLT.ABS.

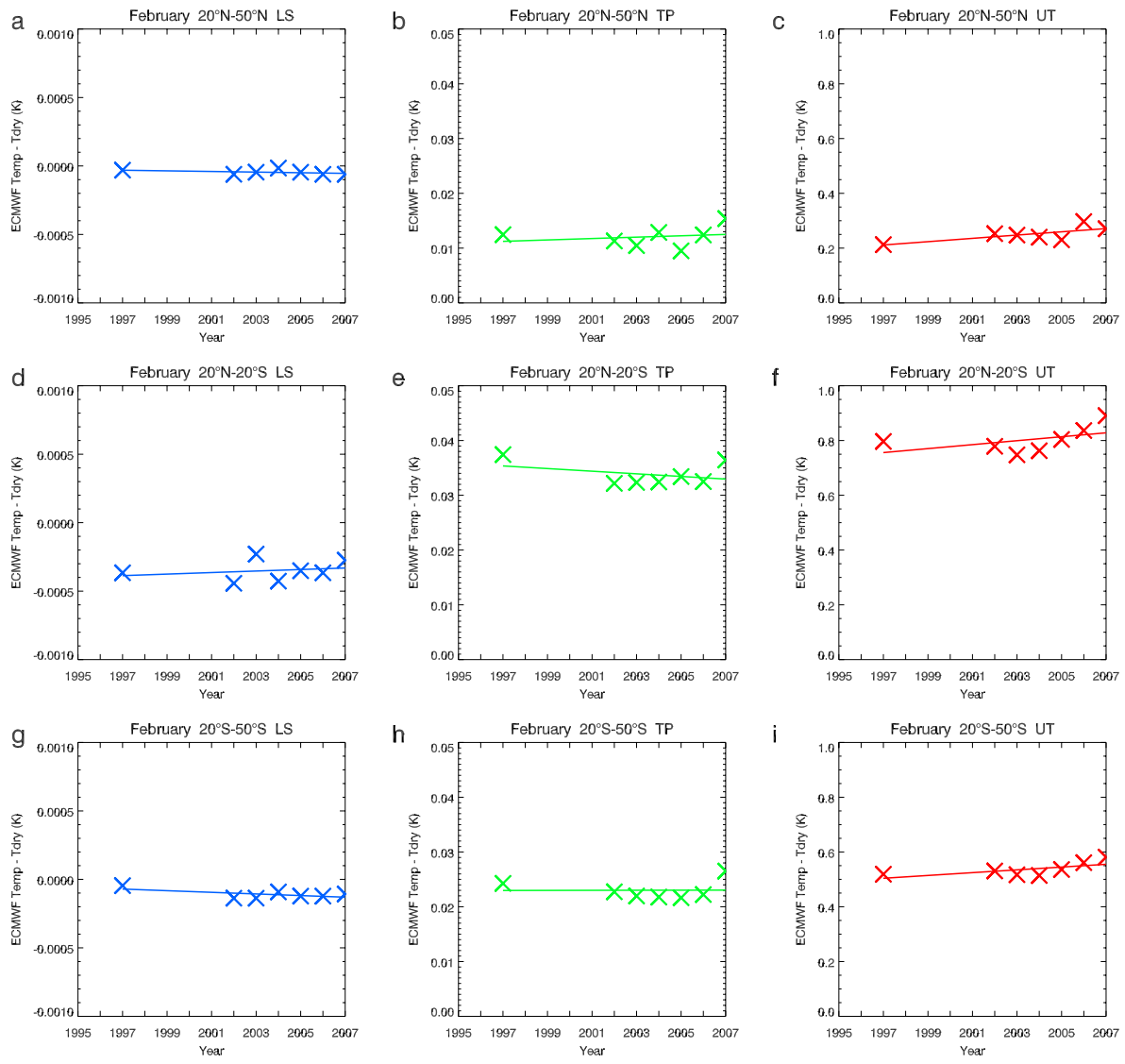

Figure S9: Trend difference of actual temperature minus dry temperature (crosses) for February 1997–2007 (straight line) based on RO-collocated profiles from ECMWF analyses (and ERA-40 in 1997), for LS (blue), TP (green), and UT (red) shown for NHE (**a**–**c**), the tropics (**d**–**f**), and SHE (**g**–**i**). Due to the small concentration of stratospheric water vapor in the LS, the difference between actual and dry temperature is < 0.01 K and becomes several 0.01 K in the tropopause region (TP). The effect of water vapor becomes important in the upper troposphere (UT) showing a difference from 0.2 K at mid-latitude winter hemisphere up to 0.9 K in the tropics. Regarding trends, the positive trend difference is consistent with an increase in specific humidity along with tropospheric warming while relative humidity remains essentially constant [*Held and Soden*, 2006]. Its impact on actual temperature is a larger warming trend than that of dry temperature resulting in a positive trend difference (of ~0.07 K/decade in the tropics). Note the different temperature axis ranges for LS, TP, and UT.

Auxiliary Tables

Table S1. Overview on time range, number of realizations, and resolution of the three GCMs selected for this study. For explanation of model acronyms see Auxiliary Data and Methods.

Global Climate Models	Time Range/No. of Realizations			Horizontal Resolution	Vertical Levels [hPa]
	PreInCtl	*SRES-A2*	*SRES-B1*		
		2001–2020	2001–2020	2.5° x 2.5°	300, 200, 150, 100, 50, 30
NCEP-NCAR/CCSM3	230 a (run1) 500 a (run2)	5	7		
MPI/ECHAM5	506 a	3	3		
UKMO/HadCM3	341 a	1	1		

Table S2. Number of radio occultation events in the investigated regions within 1995/1997–2007/2008. Note that February has 28/29 days and October 31 days.

February	**50°N–20°N**	**20°N–20°S**	**20°S–50°S**
1997	197	175	292
2002	342	280	374
2003	717	880	860
2004	795	1042	849
2005	559	954	622
2006	720	1021	742
2007	643	985	693
2008	749	730	777
October	**50°N–20°N**	**20°N–20°S**	**20°S–50°S**
1995	231	172	249
2001	214	284	272
2002	678	950	795
2003	733	1134	870
2004	660	1068	723
2005	1007	805	1053
2006	964	1025	1078
2007	644	695	663

Table S3. Overview of the Wegener Center atmospheric profiles retrieval processing scheme OPSv5.4, dry air.

Processing Step	*Description*
Early outlier rejection	"3σ" outlier rejection on 50 Hz sampling rate L1 and L2 phase delay data, based on a one-second moving average window over the profile.
Phase delay smoothing	Smoothing of 50 Hz phase delay profiles using regularization filtering (third order norm, regularization parameter = 10^5 [*Syndergaard*, 1999]).
Bending angle retrieval	Geometric optics retrieval [ref. main paper: *Kursinski et al.*, 1997] at both L1 and L2 frequencies.
Ionospheric correction	Linear combination of L1 and L2 bending angles [*Vorob'ev and Krasil'nikova*, 1994]. Correction is applied to low-pass filtered bending angles (1 km moving average), L1 high-pass contribution is added after correction [*Hocke et al.*, 2003]. L2 bending angles < 15 km derived via L1–L2 extrapolation.
Statistical optimization of bending angles	Statistical optimization of bending angles between 30 km and 120 km with inverse covariance weighting [*Healy*, 2001; *Rieder and Kirchengast*, 2001; *Gobiet and Kirchengast*, 2004]. Vertically correlated background (corr. length 10 km) and observation (corr. length 2 km) errors. Observation error estimated from variance of observed profile between 65 km and 80 km. Background error: 15 %.
	Background information: collocated profiles derived from ECMWF 24h/30h forecast files (T42L60; resp. T42L91 as of 01/02/2006), ERA-40 re-analysis for GPS/Met data. Above ~60/80 km: MSISE-90 [*Hedin*, 1991].
Abel transform to refractivity	Numerical integration over bending angle (Simpson's trapezoidal rule) from each height (impact parameter) to 120 km. Impact parameter to height conversion with radius of curvature at mean tangent point location [*Syndergaard*, 1998].
Refractivity smoothing (resolution-conserving)	Sinc-windowed Blackman filter (< 1 km moving average) for resolution-conserving filtering of residual numerical processing noise.
Hydrostatic integral, initialization for pressure	Initialization at 120 km: pressure = pressure(MSISE-90); no initialization below 120 km (downward integration).
Temperature smoothing (resolution-conserving)	Same filtering as for refractivity smoothing.
Lower cut-off altitude	The lowermost altitude, where retrieved data is kept, is set to the altitude, where significant impact parameter ambiguities occur (impact parameter increase > 0.2 km from one data point to the next downwards).
External quality control (for outlier profiles)	Refractivity 5 km to 35 km: $\Delta N/N < 10$ %; Temperature 8 km to 25 km: $\Delta T < 20$ K. Reference: collocated ECMWF analysis profiles (T42L60 resp. T42L91 as of 01/02/2006), ERA-40 re-analysis for GPS/Met data.
Reference frame, vertical coordinate	Earth figure: WGS-84 ellipsoid; Vertical coordinate: mean-sea-level (MSL) altitude; conversion of (ellipsoidal) height to MSL altitude (at mean tangent point location) via EGM-96 geoid smoothed to 2° × 2° resolution.

Auxiliary References

Angell, J. K. (2000), Tropospheric temperature variations adjusted for El Niño, 1958-1998, *J. Geophys. Res*., *105*, 11,841–11,849.

Borsche, M. *et al.* (2006), Pre-operational retrieval of radio occultation based climatologies, in *Atmosphere and Climate: Studies by Occultation Methods*, edited by U. Foelsche, G. Kirchengast, and A. K. Steiner, pp. 315–323, doi:10.1007/3-540-34121-8_26, Springer, Berlin-Heidelberg.

Borsche, M. (2008), Global atmospheric climatologies from radio occultation data and derivation of diagnostic parameters for climate monitoring, (Ph.D. thesis), *Sci. Rep. No. 22-2008*, ISBN 978-3-9502308-6-5, Wegener Center Verlag, Graz, Austria.

Collins, W. *et al*. (2006), The community climate system model version 3 (ccsm3), *J. Clim.*, *19*, 2122–2143.

Cordero, E. C., and P. M. de Forster (2006), Stratospheric variability and trends in models used for the IPCC AR4, *Atmos. Chem. Phys.*, *6*, 5369–5380.

Foelsche, U., M. Borsche, A. K. Steiner, A. Gobiet, B. Pirscher, G. Kirchengast, J. Wickert, and T. Schmidt (2008a), Observing upper troposphere–lower stratosphere climate with radio occultation data from the CHAMP satellite, *Clim. Dyn*., *31*, 49–65.

Foelsche, U., G. Kirchengast, M. Borsche, B. Pirscher, and A. K. Steiner (2008b), Creating a consistent radio occultation data base for climate studies in the upper troposphere and lower stratosphere, *Proc. of the ECMWF GRAS-SAF Workshop on Applications of Radio Occultation Measurements,* 16–18 June 2008, ECMWF, Reading, UK, 151–165.

Foelsche, U., B. Pirscher, M. Borsche, A. K. Steiner, G. Kirchengast, and C. Rocken (2009), Climatologies based on radio occultation data from CHAMP and Formosat-3/COSMIC, in *New Horizons in Occultation Research: Studies in Atmosphere and Climate*, edited by A. K. Steiner, B. Pirscher, U. Foelsche, and G. Kirchengast, pp. 179–192, Springer, Berlin Heidelberg, in press.

Gobiet, A., and G. Kirchengast (2004), Advancements of GNSS radio occultation retrieval in the upper stratosphere for optimal climate monitoring utility, *J. Geophys. Res.*, *109*, D24110, doi:10.1029/2004JD005117.

Gobiet, A., U. Foelsche, A. K. Steiner, M. Borsche, G. Kirchengast, and J. Wickert (2005), Climatological validation of stratospheric temperatures in ECMWF operational analyses with CHAMP radio occultation data, *Geophys. Res. Lett*., *32*, L12806, doi:10.1029/2005GL022617.

Gobiet, A., G. Kirchengast, G. L. Manney, M. Borsche, C. Retscher, and G. Stiller (2007), Retrieval of temperature profiles from CHAMP for climate monitoring: Intercomparison with Envisat MIPAS and GOMOS and different analyses, *Atmos. Chem. Phys.*, *7*, 3519–3536.

Gordon, C., C. Cooper, C. A. Senior, H. T. Banks, J. M. Gregory, T. C. Johns, J. F. B. Mitchell, and R. A. Wood (2000), The simulation of SST, sea ice extents and ocean heat transports in a version of the Hadley Centre coupled model without flux adjustments, *Clim. Dyn*., *16*, 147–168.

Hajj, G. A., C. O. Ao, B. A. Iijima, D. Kuang, E. R. Kursinski, A. J. Mannuci, T. K. Meehan, L. J. Romans, M. de la Torre Juarez, and T. P. Yunck (2004), CHAMP and SAC-C atmospheric occultation results and intercomparisons, *J. Geophys. Res*., *109*, D06109.

Healy, S. B. (2001), Smoothing radio occultation bending angles above 40 km, *Ann. Geophys.*, *19*, 459–468.

Hedin, A. E. (1991), Extension of the MSIS thermosphere model into the middle and lower atmosphere, *J. Geophys. Res.*, *96*, 1159–1172.
Held, I. M., and B. J. Soden (2006), Robust responses of the hydrological cycle to global warming, *J. Clim*., *19*, 5686–5699.
Hocke, K., K. Igarashi, and T. Tsuda (2003), High-resolution profiling of layered structures in the lower stratosphere by GPS occultation, *Geophys. Res. Lett.*, *30*, doi:10.1029/2002GL016566.
Intergovernmental Panel on Climate Change (2007), *Climate Change 2007: The Physical Science Basis. Contribution of Working Group I to the Fourth Assessment Report of the Intergovernmental Panel on Climate Change*, edited by S. Solomon et al., 996 pp., Cambridge Univ. Press, Cambridge, U. K.
Kirchengast, G., S. Schweitzer, J. Ramsauer, and J. Fritzer (2007), End-to-end Generic Occultation Performance Simulator version 5.2 (EGOPSv5.2) Software User Manual (Overview, Reference, and File Format Manual), *Tech. Rep. ESA/ESTEC-4/2007*, Wegener Center and IGAM, Univ. of Graz, Austria.
Kursinski, E. R., et al. (1996), Initial results of radio occultation observations of Earth's atmosphere using the global positioning system, *Science*, *271*, 1107–1110.
Leroy, S. S., J. G. Anderson, and G. Ohring (2008), Climate signal detection times and constraints on climate benchmark accuracy requirements, *J. Clim*., *21*, doi:10.1175/2007JCLI1946.1.
Luntama, J.-P., G. Kirchengast, M. Borsche, U. Foelsche, A. K. Steiner, S. Healy, A. von Engeln, E. O'Clerigh, and C. Marquardt (2008), Prospects of the EPS GRAS mission for operational atmospheric applications, *Bull. Am. Meteorol. Soc*., *89*, 1863–1875.
Meehl, G. A., C. Covey, T. Delworth, M. Latif, B. McAvaney, J. F. B. Mitchell, R. J. Stouffer, and K. E. Taylor (2007), The WCRP CMIP32 Multimodel Dataset: A new era in climate change research, *Bull. Am. Meteorol. Soc*., *88*, doi:10.1175/BAMS-88-9-1383.
Pirscher, B., U. Foelsche, B. C. Lackner, and G. Kirchengast (2007), Local time influence in single-satellite radio occultation climatologies from sun-synchronous and non sun-synchronous satellites, *J. Geophys. Res*., *112*, D11119, doi:10.1029/2006JD007934.
Pope, V., M. Galliani, P. Rowntree, and R. Stratton (2000), The impact of new physical parameterization in the Hadley Centre model: HadAM3, *Clim. Dyn*., *16*, 123–146.
Press, W. H., B. P. Flannery, S. A. Teukolsky, and W. T. Vetterling (1987), *Numerical Recipes, The Art of Scientific Computing*, Cambridge Univ. Press.
Randel, W. J., F. Wu, and W. R. Ríos (2003), Thermal variability of the tropical tropopause region derived from GPS/MET observations, *J. Geophys. Res*., *108*, doi:10.1029/2002JD002595.
Reichler, T., and J. Kim (2008), How well do coupled models simulate today's climate? *Bull. Am. Meteorol. Soc*., *89*, 303–311.
Rieder, M., and G. Kirchengast (2001), Error analysis and characterization of atmospheric profiles retrieved from GNSS occultation data, *J. Geophys. Res.*, *106*, 31,755–31,770.
Rocken, C., Y-H. Kuo, W. S. Schreiner, D. Hunt, S. Sokolovskiy, and C. McCormick (2000), COSMIC system description, *Terr. Atmos. and Oceanic Sci.*, *11*, 21–52.
Rocken, C., W. Schreiner, S. Sokolovskiy, and D. Hunt (2009), Ionospheric errors in COSMIC radio occultation profile, paper presented at the 89th American Meteorological Society Annual Meeting, Phoenix, AZ, 14 January 2009.
Roeckner, E. *et al*. (2003), The atmospheric general circulation model ECHAM5, *Rep. no. 349*, Max-Planck-Institute for Meteorology, Hamburg, Germany.

Roeckner, E., J. Jungclaus, U. Mikolajewicz, and S. Hagemann (2007), Model information of potential use to the IPCC lead authors and the AR4: ECHAM5_MPI_OM, (www-pcmdi.llnl.gov/ipcc/model_documentation/ipcc_model_documentation.php).

Schmidt, T., J. Wickert, G. Beyerle, and C. Reigber (2004), Tropical tropopause parameters derived from GPS radio occultation measurements with CHAMP, *J. Geophys. Res.*, *109*, D13105.

Seidel, D. *et al*. (2004), Uncertainty in signals of large-scale climate variations in radiosonde and satellite upper-air temperature datasets, *J. Clim*., *17*, 2225–2240.

Steiner, A. K., G. Kirchengast, M. Borsche, and U. Foelsche (2009), Lower stratospheric temperatures from CHAMP RO compared to MSU/AMSU records: An analysis of error sources, in *New Horizons in Occultation Research: Studies in Atmosphere and Climate*, edited by A. K. Steiner, B. Pirscher, U. Foelsche, and G. Kirchengast, pp. 217–232, Springer, Berlin Heidelberg, in press.

von Storch, H., and F. Zwiers (1999), *Statistical Analysis in Climate Research*, Cambridge Univ. Press, Cambridge, ed. 1.

Syndergaard, S. (1998), Modeling the impact of the Earth's oblateness on the retrieval of temperature and pressure profiles from limb sounding, *J. Atmos. Sol.-Terr. Phys.*, *60*, 171–180.

Syndergaard, S. (1999), Retrieval analysis and methodologies in atmospheric limb sounding using the GNSS radio occultation technique, *DMI Sci. Rep. 99-6*, Danish Met. Inst., Denmark.

Vorob'ev, V. V., and T. G. Krasil'nikova (1994), Estimation of the accuracy of the atmospheric refractive index recovery from Doppler shift measurements at frequencies used in the NAVSTAR system, *Phys. Atmos. Ocean*, *29*, 602–609.

Ware, R., et al. (1996), GPS sounding of the atmosphere from low Earth orbit: Preliminary results, *Bull. Am. Meteorol. Soc.*, *77*, 19–40.

Weatherhead, E. C. *et al*. (1998), Factors affecting the detection of trends: Statistical considerations and applications to environmental data, *J. Geophys. Res*., *103*, 17,149–17,161.

Weatherhead, E. C., A. J. Stevermer, and B. E. Schwartz (2002), Detecting environmental changes and trends, *Phys. Chem. Earth*, *27*, 399–403.

Wickert, J., T. Schmidt, G. Beyerle, R. König, C. Reigber, and N. Jakowski (2004), The radio occultation experiment aboard CHAMP: Operational data analysis and validation of vertical atmospheric profiles, *J. Meteorol. Soc. Japan*, *82*, 381–395.

Wickert, J., G. Beyerle, R. König, S. Heise, L. Grunwaldt, G. Michalak, C. Reigber, and T. Schmidt (2005), GPS radio occultation with CHAMP and GRACE: A first look at a new and promising satellite configuration for global atmos. sounding, *Ann. Geophys.*, *23*, 653–658.

Wickert, J., T. Schmidt, G. Michalak, S. Heise, C. Arras, G. Beyerle, C. Falck, R. König, D. Pingel, and M. Rothacher (2009), GPS radio occultation with CHAMP, GRACE-A, SAC-C, TerraSAR-X, and FORMOSAT-3/COSMIC: Brief review of results from GFZ, in *New Horizons in Occultation Res.: Studies in Atmosphere and Climate*, edited by A. K. Steiner, B. Pirscher, U. Foelsche, and G. Kirchengast, pp. 3–16, Springer, Berlin Heidelberg, in press.

Wu, B.-H., V. Chu, P. Chen, and T. King (2005), FORMOSAT-3/COSMIC science mission update, *GPS Solutions*, *9*, 111–121.

– end of document –